



Contents lists available at ScienceDirect

Acta Biomaterialia

journal homepage: www.elsevier.com/locate/actabiomat

Full length article

Concurrently suppressing multidrug resistance and metastasis of breast cancer by co-delivery of paclitaxel and honokiol with pH-sensitive polymeric micelles

Ziqi Wang, Xinru Li, Dishu Wang, Yang Zou, Xiaoyou Qu, Chuyu He, Yunqiang Deng, Yao Jin, Yuanhang Zhou, Yanxia Zhou, Yan Liu*

Beijing Key Laboratory of Molecular Pharmaceutics and New Drug Delivery Systems, School of Pharmaceutical Sciences, Peking University, Beijing 100191, China

ARTICLE INFO

Article history:

Received 9 April 2017

Received in revised form 4 August 2017

Accepted 18 August 2017

Available online xxx

Keywords:

pH-sensitive polymeric micelles

Multidrug resistance reversal

Tumor metastasis

Honokiol

Paclitaxel

Combined delivery

ABSTRACT

To concurrently suppress multidrug resistance (MDR) and metastasis of breast cancer cells, paclitaxel (PTX) and honokiol (HNK) were coencapsulated into pH-sensitive polymeric micelles based on poly(2-ethyl-2-oxazoline)-poly(D,L-lactide) (PEOz-PLA). The physicochemical properties of dual drug-loaded PEOz-PLA micelles were characterized in size, drug loading and *in vitro* release. The efficiency of MDR reversal for the micelles was testified by synergetic enhancement of cytotoxicity and uptake by MCF-7/ADR cells. The flow cytometry and fluorescence polarization measurement results reinforced the conclusion that down-regulation of P-gp expression and increase of plasma membrane fluidity appeared to be possible mechanisms of MDR reversal by dual drug-loaded PEOz-PLA micelles. Further, the efficient inhibition of tumor metastasis by dual drug-loaded PEOz-PLA micelles was demonstrated by *in vitro* anti-invasion and anti-migration assessment in MDA-MB-231 cells and *in vivo* bioluminescence imaging in nude mice. The suppression of MDR and metastasis by the micelles was assigned to synergistic effects of pH-triggered drug release and HNK/PEOz-PLA-aroused P-gp inhibition, and pH-triggered drug release and PTX/HNK-aroused MMPs inhibition, respectively. In conclusion, our findings strengthen the usefulness of co-delivery of PTX and HNK by pH-responsive polymeric micelles for suppression of tumor MDR and metastasis.

Statement of Significance

Multidrug resistance (MDR) and metastasis are considered to be two of the major barriers for successful chemotherapy. The combination of a chemotherapeutic drug with a modulator has emerged as a promising strategy for efficiently treating MDR cancer and preventing tumor metastasis. Herein, a dual drug (paclitaxel and honokiol)-loaded pH-sensitive polymeric micelle system based on PEOz-PLA was successfully fabricated to ensure that tumor MDR and metastasis could be concurrently suppressed, therefore achieving distinguishing endo/lysosomal pH from physiological pH by accelerating drug release and then enhancing the cytotoxicity of paclitaxel to drug-resistant tumor cells MCF-7/ADR by increasing cellular uptake of paclitaxel, preventing *in vitro* invasion and migration for MDA-MB-231 cells and *in vivo* metastasis in nude mice. Further, the mechanism of MDR reversal by dual drug-loaded PEOz-PLA micelles was elucidated to be down-regulation of P-gp expression and increase of plasma membrane fluidity of MCF-7/ADR cells. The present findings strengthen the usefulness of co-delivery of PTX and HNK by pH-responsive polymeric micelles for suppression of tumor MDR and metastasis.

© 2017 Acta Materialia Inc. Published by Elsevier Ltd. All rights reserved.

1. Introduction

At present, chemotherapy is still the optimal choice for cancer therapy in the clinic [1], and multidrug resistance (MDR), which is the phenomenon in which tumor cells are resistant to the cytotoxicity of chemotherapeutic drugs with various unrelated

* Corresponding author.

E-mail address: yanliu@bjmu.edu.cn (Y. Liu).

structures or action mechanisms [2,3], is considered to be one of the major barriers for successful chemotherapy. Several mechanisms have been believed to contribute to MDR including overexpression of a broad-spectrum of drug efflux transporters. The most well-known efflux transporter P-glycoprotein (P-gp) is a family member of ATP-binding cassette proteins. Overexpression of P-gp reduces intracellular accumulation of a wide range of chemotherapeutics such as paclitaxel (PTX). P-gp-mediated MDR has been observed in many tumor cell lines such as drug-resistant human breast adenocarcinoma MCF-7/ADR cells [4]. Thus, the effective way to overcome P-gp mediated MDR has been believed to either block P-gp efflux function or inhibit P-gp expression by some specific agents. A wide range of chemical modulators have been identified to inhibit P-gp efflux [5], and the combination of a chemotherapeutic drug with a P-gp inhibitor has emerged as a promising strategy for treating MDR cancer.

The clinical applications of some chemotherapeutic drugs and P-gp inhibitors were greatly restricted due to their poor water solubility or severe side effects. Thus, one of the rational and commonly used strategies to overcome MDR is to co-deliver antitumor drugs and P-gp inhibitors by nanoparticle drug delivery systems [6,7]. In the past few years, nanoscaled drug carriers have been applied to reverse MDR with the development of nanotechnology [8,9]. Among them, polymeric micelles have been received much attention and their applications are increasing due to their non-toxicity, biocompatibility, high stability, passive targeting ability through EPR effect and controlled drug release [10–12]. Further, a number of block copolymers have been demonstrated to exhibit the activity of P-gp efflux inhibition [13–15]. For example, Zou et al. implemented the coentrapment of doxorubicin and curcumin into PEG-DSPE micelles, and engineered the simultaneous release of the two drugs [16]. The release of curcumin inactivated P-gp, subsequently increasing sensitivity of tumor cells to doxorubicin, which resulted in an enhanced cytotoxicity of doxorubicin. This combination provided a novel platform for chemotherapy. Nevertheless, the premature drug release in blood circulation and slow drug release inside tumor cells still remain challenges. Thus, an efficient polymeric micelle drug delivery system is desirable.

Metastasis is another main cause for therapeutic failure in cancer treatment [17]. In many cases, metastasis has already occurred by the time tumor is detected. In general, few patients with metastatic cancer can be cured through chemotherapy, surgery and radiotherapy as the existed challenges for treating metastases including their small size, high multiplicity and dispersion to various organs [18,19]. As the biological mechanisms of metastasis are being unraveled, new approaches to treat this condition may become available. Combination therapy with more than one drug is one of the promising strategies for preventing cancer metastasis at the same time of treating cancer. The development of biomedical nanotechnology might offer a hope for this therapy [18,19]. Karaca et al. reported that methoxypoly-(ethylene)-block-poly(2-methyl-2-carboxyl-propylene carbonate) micelles carrying gemcitabine and GDC-0449 (hedgehog inhibitor) significantly inhibited the growth of pancreatic cancers and the incidence of metastasis in mice [20]. However, both premature drug release in blood circulation and slow drug release inside tumor cells are still present. Thus, novel delivery strategies are urgently needed for treatment of MDR tumor and reduction in incidence of metastasis.

pH-responsive polymeric micelles seemed to be the most attractive candidate due to the intrinsic difference in relative acidity of extracellular matrix between solid tumors and normal tissues [21]. Further, the intracellular trafficking of polymeric micelles following their internalization via endocytosis proceeds generally through the endosomal-lysosomal pathway with a pH gradient [22]. Based on these, in our previous work [12], we designed an amphiphilic block copolymer poly(2-ethyl-2-

oxazoline)-poly(D,L-lactide) (PEOZ-PLA) capable of self-assembling into pH-responsive polymeric micelles, and evidenced that PEOZ-PLA micelles could distinguish endo/lysosomal pH and tumor extracellular pH from physiological pH by accelerating drug release. This pH-dependent release behavior of the micelles may promote their tumor targeting and rapid drug release inside tumor cells, thereby significantly improving antitumor effects of antitumor drugs.

Honokiol (HNK), isolated from *Magnolia grandiflora*, has been demonstrated to be a potent anticancer drug with activity in inducing apoptosis, enhancing cell differentiation, inhibiting VEGF induced KDR autophosphorylation and repressing the growth of angiosarcoma but not a P-gp substrate. Further, HNK can reverse MDR and thereby resume the sensitivity of tumor cells to anticancer drugs by down-regulation of P-gp expression at mRNA and protein levels in various drug resistant tumor cell lines, such as MCF-7/ADR cells [23] and SKOV3 cells [24]. In addition, HNK was found to be not only active against primary tumors [25] but also effective at reducing metastases [26,27] due to its inhibition on NF- κ B activation [28], which is beneficial to enhance the efficacy of cancer chemotherapy [28]. Consequently, HNK might be a promising chemotherapeutic agent for MDR cancer and metastasis.

To exploit the therapeutic benefits that harnessed the combined delivery of PTX, a substrate for P-gp [11], and HNK, the drugs should be co-delivered to the tumor region and rapidly released in tumor cells. We have previously demonstrated that the therapeutic benefits from DOX and TPGS1000 could be enhanced through encapsulation into nanosized pH-responsive polymeric micelles [12]. In the present work, the merits of pH-sensitive PEOZ-PLA micelles for quick drug release inside tumor cells and efficient endo/lysosomal escape, and HNK for its P-gp efflux and metastases inhibition activities were integrated to fabricate dual drug-loaded PEOZ-PLA micelles for co-delivery of PTX and HNK to reverse tumor MDR and prevent metastasis. Therefore, the physicochemical properties of the dual drug-loaded polymeric micelles in terms of particle size, drug loading, pH-dependent *in vitro* release were characterized. The cytotoxicity against MCF-7/ADR cells and cellular uptake were evaluated in detail. In addition, the potential mechanisms involved in MDR reversal of dual drug-loaded PEOZ-PLA micelles were disclosed. Finally, the possibility of preventing tumor metastasis for dual drug-loaded PEOZ-PLA micelles was also evaluated *in vitro* and *in vivo*. The designed micelles were expected to be an effective delivery system for anticancer drugs and HNK to suppress tumor MDR and metastasis.

2. Materials and methods

2.1. Materials

Paclitaxel (PTX) was purchased from Guangzhou Eastbang pharmaceutical technology Co. Ltd. (Guangzhou, China). Honokiol (HNK) was obtained from the National Institute for the Control of Pharmaceutical and Biological Products (Beijing, China). 2-Ethyl-2-oxazoline supplied by Sigma-Aldrich (St Louis, MO) was dried by vacuum distillation over calcium hydride. D,L-Lactide obtained from Daigang Biological Technology Co. Ltd. (Jinan, China) was purified by recrystallization with the mixture of benzene and ethyl acetate (6:4, v/v). Sulforhodamine B sodium salt (SRB) and Matrigel were obtained from Sigma-Aldrich (St Louis, MO, USA). Dulbecco's modified Eagle medium (DMEM), fetal bovine serum (FBS), trypsin-EDTA, penicillin-streptomycin solution, 6-well, 24-well and 96-well tissue culture plates, Transwell[®] of 12-well plate, and 25 and 75 cm² plastic culture flasks were supplied by M&C Gene Technology (Beijing, China). Rhodamine 123 (R123) was purchased from Sigma (Beijing, China). TMA-DPH was acquired from

Aladdin Reagent Co., Ltd. (Shanghai, China). PE-conjugated mouse anti-human P-gp monoclonal antibody and its isotype control were obtained from BD Biosciences (NJ, USA). All other reagents and chemicals were of analytical grade or better.

2.2. Synthesis and characterization of PEOz-PLA copolymer

PEOz3300-PLA1500 diblock copolymer was synthesized through a two-step reaction as our previously reported [29].

The obtained polymers were confirmed by the ^1H NMR spectrum recorded on a Bruker MSL2300 spectrometer (400 MHz, Germany) using tetramethylsilane (TMS) as an internal reference at room temperature. The molecular weight and molecular weight distribution of the polymers were measured by gel permeation chromatography (GPC, Spectra System P100) with a refractive index detector (RefractoMonitor IV) by using polystyrene as standards.

Acid dissociation constant ($\text{p}K_a$) of the synthesized polymers was determined by acid-base titration with sodium hydroxide as previously reported [12].

The critical micelle concentration (CMC) of the copolymer was measured by a fluorescence technique with pyrene as a hydrophobic probe as described previously [30].

2.3. Preparation of drug-loaded polymeric micelles

Single drug-loaded PEOz-PLA micelles (denoted as PTX/PP-PM and HNK/PP-PM, respectively) were prepared by film-hydration method [31]. Briefly, PEOz-PLA (20.0 mg) and drug (1.0 mg) were dissolved in methanol (10 mL) followed by removal of methanol through rotary evaporation under reduced pressure at 40 °C to form a thin film. 10 mL of ultra-pure water was added to hydrate the thin film at 60 °C and then vortexed for 5 min. Nonencapsulated insoluble drugs were removed by filtration of the micelle suspension through a membrane filter (0.22 μm) to obtain a clear and homogeneous micelle solution. The resultant micelle solutions were freeze-dried for further characterizations.

R123-loaded PEOz-PLA micelles (denoted as R123/PP-PM) were prepared by film hydration method as described above except that drug (1.0 mg) was replaced by R123 (19 μg).

Dual drug-loaded PEOz-PLA micelles (denoted as PTX+HNK/PP-PM1 for 1:1 mass ratio of PTX to HNK and PTX+HNK/PP-PM2 for 2:1 mass ratio of PTX to HNK, respectively) were prepared by film hydration method as described above except that drug (1.0 mg) was replaced by 1.0 mg PTX along with 1.0 mg or 0.5 mg HNK, respectively.

2.4. Physicochemical characterization of polymeric micelles

The size and size distribution of polymeric micelles were determined by dynamic light scattering (DLS) (Zetasizer nano series, Malvern, UK). All DLS measurements were performed with a scattering angle of 90° at 25 °C after micelle lyophilized powder was dispersed in an appropriate volume of deionized water.

The morphology of micelles was observed using a transmission electron microscope (TEM, JEM-1230, JEOL, Japan) as previously reported [31].

To determine the drug loading content (LC, w/w, %) and encapsulation efficiency (EE, w/w, %) of micelles, the lyophilized powder of drug-loaded micelles was dissolved in acetonitrile, and the drug content was measured by HPLC at the wavelength of 227 nm. The solution was properly diluted prior to HPLC analysis. The HPLC system (Shimadzu LC-10AT, Kyoto, Japan) was equipped with a UV detector (Shimadzu SPD-10A) and reversed phase column (Diamonsil C18, 4.6 mm \times 250 mm, Dikma Technologies, China). The mobile phase pumped at a flow rate of 1.0 mL/min was a mixed

solution of acetonitrile and water (3:1, v/v). The column temperature was set to 25 °C. The retention time of PTX and HNK was 5 min and 7 min, respectively. The LC and EE were calculated using the following equations:

$$\text{LC (\%)} = \frac{\text{mass of drug extracted from lyophilized micelles}}{\text{mass of lyophilized micelles}} \times 100,$$

$$\text{EE (\%)} = \frac{\text{mass of drug extracted from lyophilized micelles}}{\text{mass of feed PTX or HNK}} \times 100.$$

2.5. In vitro release study

In vitro release behaviors of PTX and HNK from the micelles were evaluated using a dialysis diffusion technique [32]. In total, 1 mL of drug-loaded PEOz-PLA micelle solution was transferred into a dialysis bag (MWCO 3500). Then the sealed bag was immersed into 40 mL of PBS (pH 5.0 or 7.4) containing 0.2% Tween 80 (w/w) that was kept at 37 \pm 0.5 °C with continuously shaking at 100 rpm. At predetermined time intervals, 1 mL of the release medium was withdrawn and immediately replaced with the same volume of fresh medium. The amount of released PTX and HNK in the medium was determined by use of HPLC method as described earlier and the percentage of released drugs was plotted against time.

2.6. Cell culture

Human breast cancer cell line MCF-7/ADR, MDA-MB-231 and the luciferase and green fluorescent protein-labeled MDA-MB-231 (MDA-MB-231-luc-GFP) were obtained from the China Infrastructure of Cell Line Resources (Beijing, China) and cultured in DMEM supplemented with 10% FBS at 37 °C in 5% CO₂ humidified atmosphere.

2.7. Cellular uptake assay

The cellular uptake was measured by flow cytometry as previously reported [12]. In brief, MCF-7/ADR cells were seeded into 6-well plates (3 \times 10⁵ cells/well) and cultured for 24 h at 37 °C under 5% CO₂. After that, the medium was replaced by the fresh medium (with 10% FBS) containing various micelle formulations in a series of concentration of drug. Cells treated with DMEM containing FBS were used as the negative control. Following incubation for 24 h or 36 h, the cells were washed twice with cold PBS, and then incubated with the FBS-free medium containing various R123-loaded PEOz-PLA micelles for 2 h. After being trypsinized and harvested with 0.4 mL of 0.2% (w/v) trypsin-0.1% (w/v) EDTA solution, the cells were washed and re-suspended in 0.5 mL of PBS followed by filtration through a nylon mesh. The uptake of R123 by the cells was measured by FAScan flow cytometer (Becton Dickinson FACS Calibur, Mountain View, USA).

2.8. In vitro cytotoxicity assessment

The SRB assay was used to evaluate the cytotoxicity of PTX/PP-PM, HNK/PP-PM and PTX+HNK/PP-PM [33]. Briefly, MCF-7/ADR or MDA-MB-231 cells were seeded in 96-well plates at a density of 5 \times 10⁴ cells/well and cultured for 24 h in a 5% CO₂ humidified atmosphere at 37 °C. After removing medium, 200 μL of sample solutions (PTX/PP-PM, HNK/PP-PM and PTX+HNK/PP-PM solutions in fresh serum-free medium) or negative control (serum-free DMEM) was added. After incubation for 60 h, the medium was

removed and the cells were washed once by cold PBS followed by fixing with 200 μL of 10% trichloroacetic acid (TCA) at 4 $^{\circ}\text{C}$ for 1 h. TCA was then removed and the cells were washed five times with deionized water, dried at 37 $^{\circ}\text{C}$. After the cells were stained with 100 μL of 4% (w/v) SRB in 1% (v/v) acetate solution for 30 min at room temperature, SRB was removed and the cells were washed five times with 1% (v/v) acetate solution before dried at 37 $^{\circ}\text{C}$. Then 96-well plates were shaken for 30 min at 37 $^{\circ}\text{C}$ after 150 μL of 10 mmol/L Tris was added into each well. The absorbance of each well was measured at 540 nm with a microplate reader (Bio-Rad model 550, USA). The relative cell viability was calculated according to the following equation:

$$\text{Relative cell viability (\%)} = \frac{\text{Absorbance}_{\text{test}}}{\text{Absorbance}_{\text{control}}} \times 100.$$

2.9. Measurement of P-gp level

The P-gp level in MCF-7/ADR cells was determined by flow cytometry [23]. In brief, MCF-7/ADR cells were seeded into 6-well plates at a density of 3×10^5 /well and incubated in a humidified CO_2 incubator. After incubation for 24 h, the cells were exposed to free HNK, HNK/PP-PM, and blank PEOz-PLA micelles (PP-PM) solution in DMEM with 10% FBS for 48 h. Specifically, the free HNK solution in DMEM was prepared by first dissolving HNK in a small amount of DMSO and then diluting with DMEM. Our preliminary test demonstrated that this amount of DMSO had no cytotoxicity to the cells. The final concentration for HNK was 12 $\mu\text{g}/\text{mL}$, and PEOz-PLA was 240 $\mu\text{g}/\text{mL}$, respectively. Then the cells were trypsinized, washed twice with cold PBS, labeled with PE-conjugated mouse anti-human monoclonal antibody against P-gp according to manufacturer's instruction and the non-specific labeling was corrected by its isotype control. The fluorescent intensity in cells was analyzed using a flow cytometer (FACS Caliber, Beckton Dickinson, CA, USA). Free HNK and DMEM were used as positive and blank controls, respectively.

2.10. Determination of plasma membrane fluidity

The fluorescent probe TMA-DPH, which is distributed to the lipid-water interface due to its charged moiety and thereby reflects only the interfacial region of the membrane, was used to evaluate the effect of tested samples on plasma membrane fluidity [34]. MCF-7/ADR cells were suspended in medium with free HNK, HNK/PP-PM and PP-PM (final concentration: 0.053 mg/mL (0.20 mM) for HNK, 1.06 mg/mL for PEOz-PLA) at a density of approximately 3×10^5 cells/mL. After incubation for 48 h, the medium was removed and the cells were incubated with 2 μM of TMA-DPH for 2 min at 37 $^{\circ}\text{C}$ in the dark to label cell membranes, washed twice with PBS. The fluorescent polarization (P) of MCF-7/ADR cell membrane was measured by Multiscan Spectrum (Flex Station 3, Molecular Devices) at the excitation wavelength of 365 nm and the emission wavelength of 454 nm. Membrane microviscosity of the cells were calculated using the formula: $\eta = 2P/(0.46 - P)$ [35]. Treatment of benzyl alcohol (final concentration 30 mM), documented to increase membrane fluidity, was used as a positive control. Cells treated with DMEM were served as a negative control.

2.11. Invasion assay

The cell invasion ability was evaluated using a Transwell of 24-well tissue-culture plates with 8- μm -diameter pores of polycarbonate membranes [36]. The polycarbonate membrane was coated beforehand with 80 μL of Matrigel (12.5 $\mu\text{g}/\text{mL}$) in FBS-free L-15

Leibovitz media for 30 min at 37 $^{\circ}\text{C}$. Then 0.2 mL of MDA-MB-231 cell suspensions (5×10^5 cells/mL, diluted in FBS-free L-15 Leibovitz) and 0.2 mL of PTX/PP-PM, HNK/PP-PM and PTX+HNK/PP-PM1 solution in FBS-free Leibovitz-15 were added into the upper chamber, respectively. The final concentration of HNK and PTX ranged from 0.42 $\mu\text{g}/\text{mL}$ to 6.66 $\mu\text{g}/\text{mL}$, respectively. Cells treated with FBS-free Leibovitz-15 was served as control. The lower chamber was filled with 0.5 mL of Leibovitz-15 supplemented with 10% FBS. Following incubation for 48 h in a CO_2 incubator, the cells that invaded to the lower surface of the filter were fixed, stained and counted as described in migration assay.

2.12. Evaluation of cell migration

The cell migration ability was assessed using a Transwell of 24-well tissue-culture plates with 8- μm -diameter pores of polycarbonate membranes. MDA-MB-231 cells at a density of 5×10^5 /well were put into the upper chamber, and then 0.2 mL of PTX/PP-PM, HNK/PP-PM and PTX+HNK/PP-PM1 solution in L-15 Leibovitz with 1% FBS with the final concentration of HNK and PTX ranging from 0.42 $\mu\text{g}/\text{mL}$ to 6.66 $\mu\text{g}/\text{mL}$ were added, respectively. Cells treated with L-15 Leibovitz with 1% FBS was served as control. While 0.5 mL of L-15 Leibovitz with 10% FBS was added to the lower chamber. After 48 h of incubation, the non-invading cells were removed from the upper chamber with a cotton swab, the cells in the lower chamber that had migrated to the bottom of the Transwell were fixed with methanol for 30 s, followed by staining for 30 min using 0.1% crystal violet solution in methanol [37]. The migrated cells in the lower chamber were counted with microplate reader at 570 nm. The percentage of cell migration was calculated according to the following equation:

$$\text{Cell migration (\%)} = \frac{\text{Absorbance}_{\text{test}}}{\text{Absorbance}_{\text{control}}} \times 100.$$

2.13. Evaluation of pulmonary metastasis inhibition

Normal male BALB/c nude mice (6–8 weeks old) were obtained from Animals Center of Peking University Health Science Center. All care and handling of animals were performed with the approval of Institutional Authority for Laboratory Animal Care of Peking University. Pulmonary metastasis inhibition for various micelle formulations was evaluated according to previous document with a little modification [38]. In brief, MDA-MB-231-luc-GFP cell suspension was injected into the tail vein of the nude mice at 1.5×10^6 cells per mouse in 100 μL FBS-free DMEM. After injection of tumor cells, all mice were randomly assigned to four groups ($n = 5$) and received intravenous injection of PTX/PP-PM, HNK/PP-PM, PTX+HNK/PP-PM1 and normal saline via tail vein at PTX dose of 25 mg/kg body weight and/or at HNK dose of 25 mg/kg body weight at 8 h, 5 d and 10 d for a total of three treatments, respectively. At 15th day after xenograft, to access bioluminescence, the mice received D-luciferin potassium salt stock solution (15 mg/mL) in PBS at a dose of 150 mg/kg via intraperitoneal injections. All mice were immediately anesthetized with 2% isoflurane, and imaged using an In-vivo FX multimodal imaging system (Carestream Health, USA) 10 min after luciferin injection [39]. The bioluminescent signal was quantified in the region of interest by using the *in vivo* imaging software. Afterwards, the mice were sacrificed and the lungs were isolated, weighed and *ex vivo* imaged, and then fixed in a 4% paraformaldehyde solution overnight and processed for paraffin sections followed by H&E stain, and observed by light microscopy.

2.14. Statistical analysis

All data were presented as mean \pm SD unless particularly outlined. The statistical significance of differences among more than two groups was determined by a one-way ANOVA. A p -value of 0.05 or less was considered to be statistically significant.

3. Results

3.1. Synthesis and characterization of PEOz-PLA

PEOz-OH was first synthesized by the cationic ring-opening polymerization of EOz and confirmed by ^1H NMR spectrum in CDCl_3 (Fig. S1A). The sharp peaks at 2.32 ppm and 1.03 ppm were attributed to methylene and methyl protons in the side chains, respectively. The peak at 3.37 ppm was assigned to the methylene protons in the backbone. Expanding the spectrum, there was also a little peak at 2.95 ppm that contributed to the methyl in the end of the copolymer. The number average molecular weight of PEOz-OH determined by GPC was 3300 g/mol with 1.25 of PDI. Then, diblock copolymer PEOz-PLA was synthesized by anionic ring-opening polymerization from PEOz-OH and D,L-lactide. In the ^1H NMR spectrum (Fig. S1B), the characteristic chemical shifts corresponding to PLA (5.14 ppm and 1.54 ppm) and PEOz-OH (3.44 ppm and 1.09 ppm) blocks were observed, which were in agreement with our previous report [29]. The number average molecular weight of PEOz-PLA determined by GPC was 4800 g/mol with 1.39 of PDI, implying that the obtained PEOz-PLA had well-controlled M_n with narrow distribution.

The pK_a of the synthesized PEOz-OH3300 and PEOz3300-PLA1500 were determined to be 6.4 and 6.9, respectively (Fig. S2).

The CMC of the synthesized PEOz3300-PLA1500 was determined to be 13.9 mg/L, implying that PEOz-PLA micelles might exhibit a relatively high stability in systemic circulation as drug delivery carriers.

3.2. Physicochemical characterization of polymeric micelles

A series of drug-loaded PEOz-PLA micelles were prepared and characterized by their mean size and size distribution (polydispersity index, PDI), morphology and drug loading content (LC) as well as encapsulation efficiency (EE). As shown in Fig. 1 and Table 1, the size of all prepared PEOz-PLA micelles was in the range of 41–44 nm in diameter with a narrow distribution (PDI < 0.3) and without significant difference between any two ($p > 0.05$), indicating that these micelles were stable and beneficial for passively tumor-targeted delivery of drugs loaded in micelles through enhanced permeability and retention (EPR) effect [40] and exhibited favorable stability [41]. TEM images provided a direct evidence for the formation of PEOz-PLA micelles with a well-defined spherical shape and uniform size (Fig. 1F–H). Furthermore, dual drug-loaded micelles PTX+HNK/PP-PM showed a general trend in reduction of LC and EE for each drug compared with single drug-loaded micelles PTX/PP-PM and HNK/PP-PM, implying the successful construction of dual drug-loaded polymeric micelles on the other hand. A schematic diagram depicting the self-assembly and drug loading of dual drug-loaded micelles was shown in Fig. 1A.

3.3. *In vitro* drug release from the micelles

As known, it is important to reveal the release behaviors of the encapsulated drugs from micelles for understanding the porosity of micelles and the interaction between the drug and inner core of micelles, and for guiding the design of micelles. The *in vitro*

release behavior of PTX and HNK from the dual drug-loaded PEOz-PLA micelles at 37 °C was therefore investigated in PBS with different pH value using a dialysis method. PBS (pH 7.4) was used to mimic the blood environment and PBS (pH 5.0) to stimulate endo/lysosome circumstance. As shown in Fig. 2A–D, the *in vitro* release behavior of PTX+HNK/PP-PM exhibited a biphasic pattern characterized with relative fast drug release and sustained drug release at both of pH values, in other words, both of drugs were released faster in the initial state followed by a slower continuous release over 48 h. Moreover, the release of both drugs was found to be pH-dependent and was accelerated with decrease of pH value, suggesting that the prepared PTX+HNK/PP-PM could distinguish endo/lysosomal pH from physiological pH by accelerating drug release and acidic environment is beneficial to drug release. In addition, PTX+HNK/PP-PM1 and PTX+HNK/PP-PM2 exhibited almost the same release behavior. Noticeably, the pH-dependence of PTX release was superior to that of HNK release, and the release of PTX seemed to be highly faster than that of HNK at both pH values. Specifically, for PTX+HNK/PP-PM1, for example, the release of PTX was about 57% at pH 7.4 and 74% at pH 5.0 within the first 36 h, respectively, and the PTX release curve reached a plateau thereafter. As for HNK, the release amount was about 42% at pH 7.4 and 50% at pH 5.0 within the first 36 h, respectively, and the release was sustained thereafter. These might be due to the lower solubility parameter of HNK ($18.64 \text{ J}^{1/2} \text{ m}^{-3/2}$) than PTX ($28.34 \text{ J}^{1/2} \text{ m}^{-3/2}$) calculated by the group contribution method [42], thus HNK is more lipophilic and exhibits a greater affinity to the hydrophobic inner core of the micelles.

In addition, the effect of pH values on the release behavior of PTX and HNK from the single drug-loaded PEOz-PLA micelles was also investigated for comparison. As shown in Fig. 2E, the accumulative release of PTX increased from about 55% at pH 7.4 to about 80% at pH 5.0 within 24 h, and the PTX release curve reached a plateau thereafter. Fig. 2F showed that at pH 7.4, about 48% HNK was released within 24 h, while in acidic solution (pH 5.0), the release amount increased to about 58%. Afterwards, the release amount slightly increased. Thus, similar to the situation of the dual drug-loaded micelles, the release of PTX from the single drug-loaded micelles was highly more dependent on pH value than that of HNK. Furthermore, the release of PTX (Fig. 2E) and HNK (Fig. 2F) from the single drug-loaded micelles was highly dependent on pH value and the release rate was faster compared with the dual drug-loaded micelles. A possible explanation for such difference might be attributed to the fact that the existence of HNK induced slow diffusion of PTX from the dual drug-loaded micelles, and vice versa.

3.4. Optimization of incubation time and effective concentration of HNK

In order to determine the incubation time and effective concentration of HNK in micelles, the fluorescent dye R123, a P-gp substrate, was selected as a fluorescent probe for evaluating the effect of incubation time and concentration of HNK on the P-gp-mediated drug efflux. As shown in Fig. 3A, no remarkable increase in cellular uptake of R123 loaded in PEOz-PLA micelles was observed after 24 h incubation of HNK/PP-PM with MCF-7/ADR cells in the whole HNK concentration range of 1.09–8.73 $\mu\text{g}/\text{mL}$. The similar situation was also observed after 36 h incubation of HNK/PP-PM at HNK concentration below 2.41 $\mu\text{g}/\text{mL}$, while the uptake of R123 was dramatically increased at HNK concentration above 2.41 $\mu\text{g}/\text{mL}$. These results indicated that the incubation time of HNK/PP-PM with MCF-7/ADR cells was at least 36 h and HNK worked at concentrations of greater than 2.41 $\mu\text{g}/\text{mL}$.

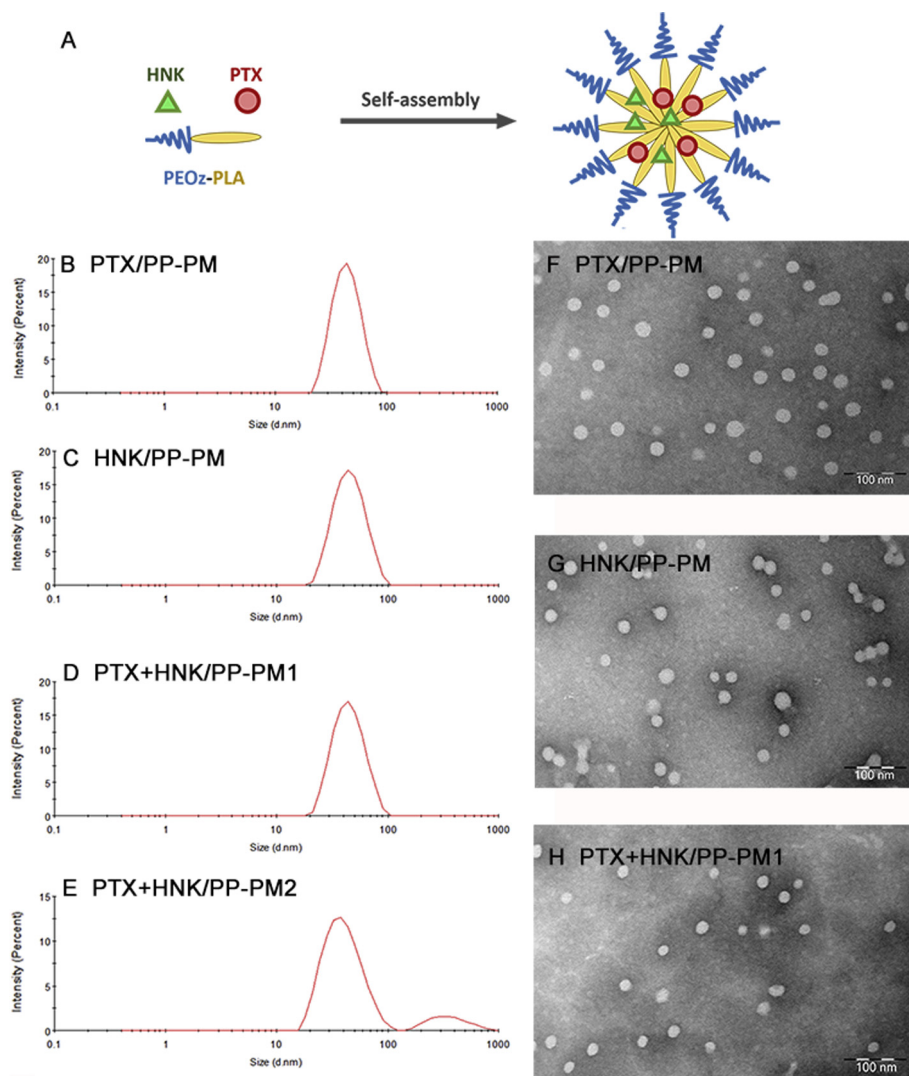


Fig. 1. (A) Schematic illustration of self-assembly for dual drug-loaded PEOz-PLA micelles in aqueous medium. Size (B, C, D, E) and transmission electron microscope images (F, G, H) of single drug-loaded PEOz-PLA micelles (B, C, F, G) and dual drug-loaded PEOz-PLA micelles (D, E, H).

Table 1
Physicochemical characteristics of drug-loaded PEOz-PLA micelles ($n = 3$).

Micelles	Diameter (nm)	PDI	LC (%)		EE (%)	
			PTX	HNK	PTX	HNK
PTX/PP-PM	41.83 ± 3.55	0.07 ± 0.01	5.0 ± 0.1	/	99.5 ± 0.2	/
HNK/PP-PM	42.72 ± 5.74	0.09 ± 0.03	/	4.1 ± 0.1	/	81.5 ± 1.0
PTX+HNK/PP-PM1	44.12 ± 4.52	0.18 ± 0.02	4.2 ± 0.7	3.6 ± 0.3*	90.5 ± 8.5 ^{ns}	79.6 ± 7.6
PTX+HNK/PP-PM2	42.13 ± 2.91	0.29 ± 0.05	4.0 ± 1.3	2.0 ± 0.9*	84.4 ± 4.3 ^{**}	83.6 ± 7.9

* $p < 0.05$ vs. HNK/PP-PM.

^{ns} $p > 0.05$.

^{**} $p < 0.05$ vs. PTX/PP-PM.

3.5. *In vitro* cytotoxicity against MCF-7/ADR cells

In order to determine the toxic concentration of HNK, a preliminary evaluation of cytotoxicity of HNK/PP-PM against P-gp over-expressing MCF-7/ADR cells was conducted using SRB assay. As shown in Fig. 3B, a relative cell viability ranging from (99.5 ± 11.5)% to (100.0 ± 7.92)% was observed for HNK/PP-PM below 14.31 µg/mL of HNK concentration, whereas the cell viability dramatically decreased thereafter. Thus, it was concluded that the cytotoxicity of HNK/PP-PM could be ignored at HNK concentra-

tion lower than 14.31 µg/mL. The IC₅₀ value of HNK/PP-PM was 24.46 ± 2.13 µg/mL (Table 2).

Next, the cytotoxicity of PTX/PP-PM and PTX+HNK/PP-PM against MCF-7/ADR cells were evaluated, respectively. As shown in Fig. 3C, the cytotoxicity of various tested micelle formulations against MCF-7/ADR cells presented evident PTX and HNK concentration-dependence. Further, for better understanding the effect of different micelle formulations on cell growth, the IC₅₀ value, a drug concentration at which 50% cells are killed, was calculated by logistic nonlinear regression and listed in Table 2. As

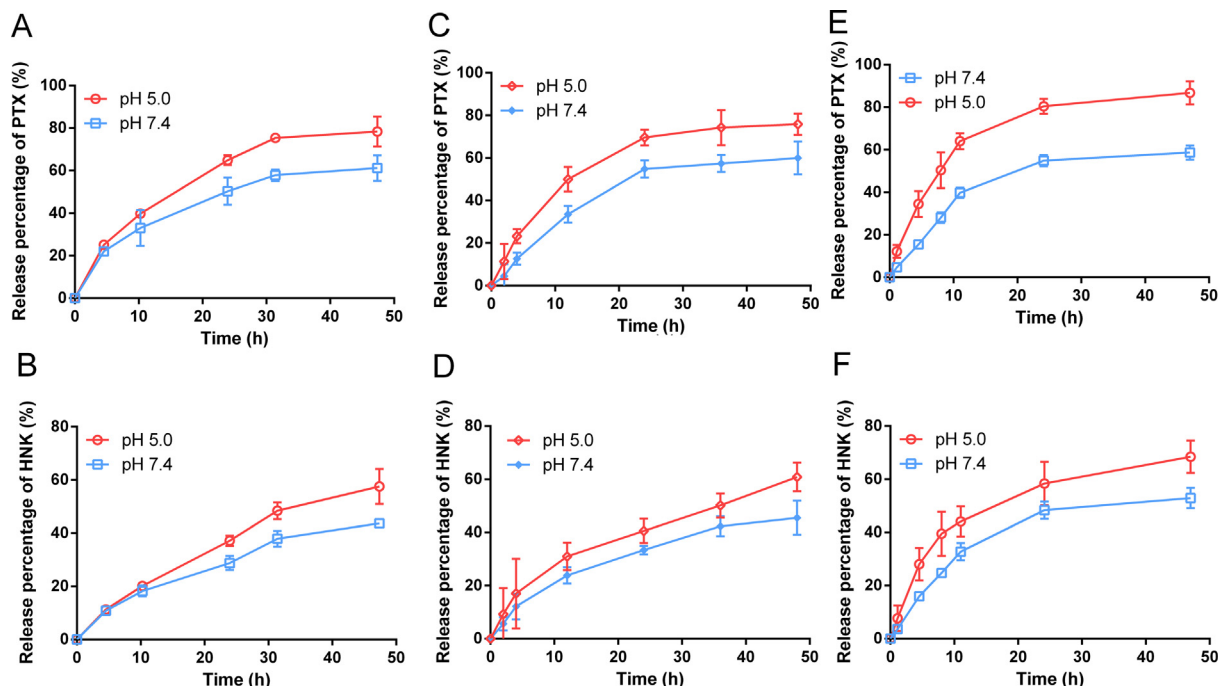


Fig. 2. *In vitro* release profiles of PTX (A, C, E) and HNK (B, D, F) from dual drug-loaded PEOz-PLA micelles PTX+HNK/PP-PM1 (A, B) and PTX+HNK/PP-PM2 (C, D), and single drug-loaded PEOz-PLA micelles (E, F) in PBS containing 0.2% Tween 80 at different pH values at 37 °C ($n = 3$).

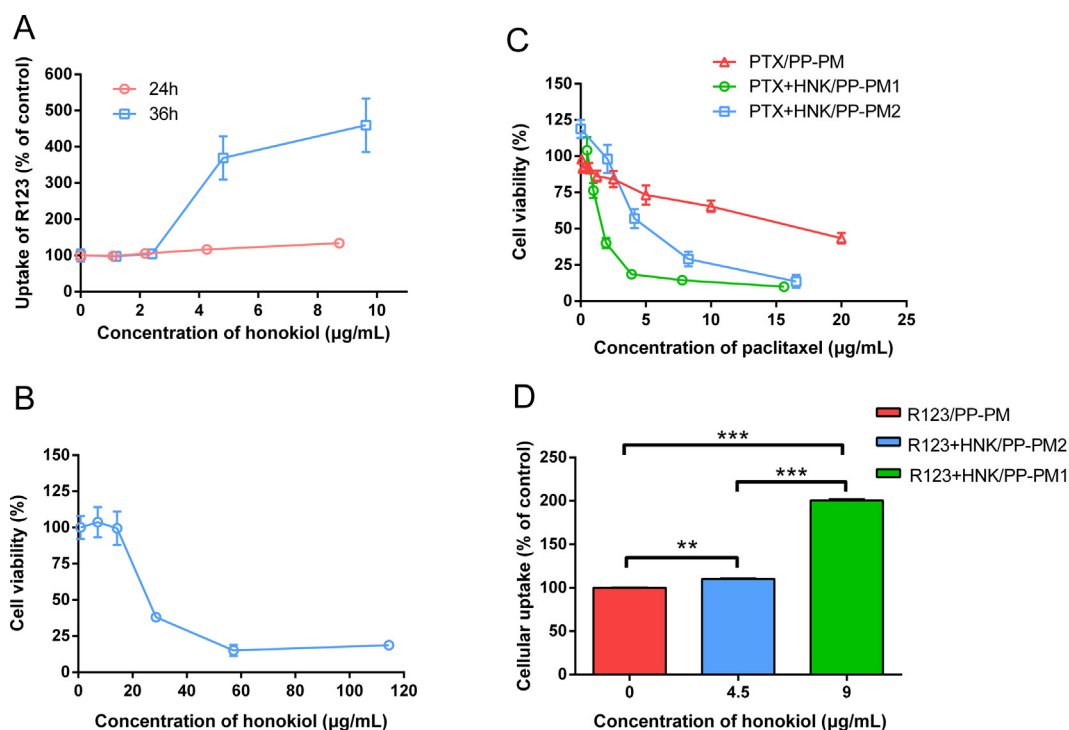


Fig. 3. (A) R123 uptake by MCF-7/ADR cells after 4 h incubation of R123/PP-PM following 24 h and 36 h incubation of HNK/PP-PM with a series of HNK concentrations. Cytotoxicity of HNK/PP-PM (B), PTX/PP-PM and PTX+HNK/PP-PM (C) against MCF-7/ADR cells after incubation for 60 h ($n = 6$). (D) R123 uptake by MCF-7/ADR cells for R123/PP-PM and R123+HNK/PP-PM after incubation for 4 h following 36 h incubation of HNK/PP-PM with the cells at 37 °C. The final concentration of R123 was 5 μM for all micelle formulations ($n = 6$). ** $p < 0.01$, *** $p < 0.001$.

reflected by IC_{50} value, the cytotoxicity of PTX+HNK/PP-PM1 and PTX+HNK/PP-PM2 was highly significantly increased compared with PTX/PP-PM ($p < 0.01$), respectively, which might be explained by the increase in cellular uptake of PTX regardless of slow release of PTX from PTX+HNK/PP-PM. In addition, the IC_{50} value of PTX

+HNK/PP-PM1 was significantly lower than that of PTX+HNK/PP-PM2 ($p < 0.01$), which might be presumably assigned to incomplete inhibition of P-gp overexpressed in MCF-7/ADR cells by insufficient amount of HNK for PTX+HNK/PP-PM2. Noticeably, the concentration of HNK was around 1.75 $\mu\text{g}/\text{mL}$ for PTX+HNK/PP-PM1 and

Table 2

IC₅₀ and RRI values of various micelle formulations against MCF-7/ADR cells by SRB assay (*n* = 6).

Micelle formulations	IC ₅₀ (μg/mL)	RRI	CI
HNK/PP-PM	24.46 ± 2.13	/	/
PTX/PP-PM	18.10 ± 1.22	/	/
PTX+HNK/PP-PM1	1.75 ± 0.19 ^a	10.34	0.168
PTX+HNK/PP-PM2	5.82 ± 0.60 ^{a,b}	3.11	0.442

^a *p* < 0.001 vs. PTX/PP-PM.

^b *p* < 0.001 vs. PTX+HNK/PP-PM1.

2.91 μg/mL for PTX+HNK/PP-PM2 at their IC₅₀, respectively, which were remarkably lower than the toxic concentration of HNK obtained from Fig. 3B, suggesting that HNK only acted as a P-gp inhibitor and could enhance the cytotoxicity of PTX against MCF-7/ADR. To gain a better view of the ability of HNK to enhance the cytotoxicity of PTX, the combination index (CI) was calculated according to the median-effect principle as follows [43]:

$$CI = \frac{D_{PTX}}{D_{x(PTX)}} + \frac{D_{HNK}}{D_{x(HNK)}}$$

where $D_{x(PTX)}$ and $D_{x(HNK)}$ are the individual dose of PTX and HNK required to inhibit a given level of cell growth, and D_{PTX} and D_{HNK} are the dose of PTX and HNK necessary to produce the same effect in combination, respectively. As expected, the CI for PTX+HNK/PP-PM1 was calculated to be 0.168 (Table 2), which was in the range of 0.1–0.3, suggesting that there existed a strong synergistic effect between PTX and HNK [44]. Whereas the CI for PTX+HNK/PP-PM2 was 0.442, which was between 0.3 and 0.7, implying that only synergism was developed between PTX and HNK.

In addition, in order to quantitatively evaluate the reversal effect on MDR by PTX+HNK/PP-PM, the resistance reversion index (RRI), which was defined as the ratio of IC₅₀ of PTX/PP-PM to that of PTX+HNK/PP-PM in the present study, was calculated. As shown in Table 2, the RRI (10.34) of PTX+HNK/PP-PM1 was about 3.3-fold higher than that (3.11) of PTX+HNK/PP-PM2, suggesting that PTX+HNK/PP-PM1 in the present study had relatively stronger MDR reversal effect and the more the content of HNK, the stronger the MDR reversal effect of PTX+HNK/PP-PM. However, the mass ratio of PTX to HNK in micelles was not arbitrary. In our preliminary test, it was found that the encapsulation efficiency of the two drugs was reduced to about 50% when the mass ratio of PTX to HNK was 1:2.

3.6. In vitro cellular uptake

Flow cytometry was used to evaluate the total cellular uptake of R123, employed as the marker for intracellular tracing, by MCF-7/ADR cells for both single drug-loaded and dual drug-loaded PEOz-PLA micelles. Prior to exposure of dual drug-loaded micelles to MCF-7/ADR cells, HNK/PP-PM was incubated with the cells for 36 h. As presented in Fig. 3D, the cellular uptake of R123 for R123+HNK/PP-PM1 (R123/HNK = 1:1) and R123+HNK/PP-PM2 (R123/HNK = 2:1) was about 2.0-fold and 1.1-fold higher than that for R123/PP-PM, respectively, which was assigned to the modulation of MDR by HNK. Further, cellular uptake of R123 for R123+HNK/PP-PM1 was extremely significantly greater than that for R123+HNK/PP-PM2 (*p* < 0.001). Therefore, co-delivery of PTX and HNK, especially by PTX+HNK/PP-PM1, may evidently enhance the uptake of PTX by MCF-7/ADR cells, suggesting that PTX+HNK/PP-PM1 in the present study could efficiently deliver PTX to MCF-7/ADR cells and thereby had significant MDR reversal effect. Therefore, PTX+HNK/PP-PM1 appeared to be the most effective micelle formulation in the present study for reversing MDR, thereby was

selected as the favorable dual drug-loaded PEOz-PLA micelles in the subsequent studies.

3.7. Effect of HNK/PP-PM on P-gp level

To evaluate the effect of HNK/PP-PM on P-gp level in MCF-7/ADR cells, MCF-7/ADR cells were incubated with HNK/PP-PM for 48 h. As shown in Fig. 4A, HNK as positive control, similar to the published report [23], significantly decreased P-gp expression in MCF-7/ADR cells to 86% following incubation for 48 h compared with blank control (*p* < 0.01). Further, significant reduction in P-gp level in MCF-7/ADR cells to 81% of the blank control was also observed for treatment with HNK/PP-PM for 48 h (*p* < 0.01), although there was no significant difference in reduction in P-gp level between HNK/PP-PM and free HNK (*p* > 0.05). By comparison,

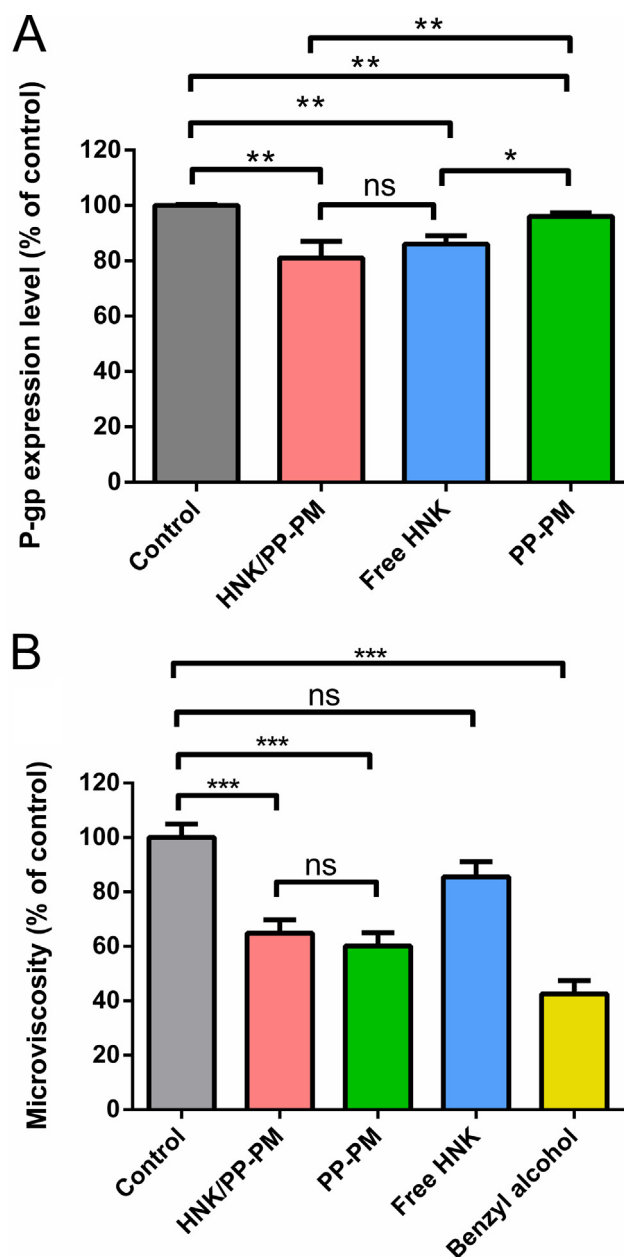


Fig. 4. (A) P-gp expression level (% of control) in the presence of free HNK, HNK/PP-PM and PP-PM, respectively (*n* = 6). (B) Variations of plasma membrane microviscosity (% of control) in MCF-7/ADR cells in the presence of free HNK, HNK/PP-PM and PP-PM (*n* = 6). ^{ns}*p* > 0.05, ^{*}*p* < 0.05, ^{**}*p* < 0.01, ^{***}*p* < 0.001.

the effect of PP-PM at a PEOz-PLA concentration equivalent to HNK/PP-PM on P-gp level was also evaluated. The result indicated that PEOz-PLA itself could significantly decrease the expression of P-gp compared with the blank control ($p < 0.01$), however, the effect of PEOz-PLA on P-gp expression in MCF-7/ADR cells was significantly inferior to that of free HNK ($p < 0.05$) and HNK/PP-PM ($p < 0.01$). Thus, it could be concluded that both free HNK and HNK/PP-PM could down-regulate P-gp expression in MCF-7/ADR cells and the effect of HNK/PP-PM was slightly superior to free HNK. In addition, PEOz-PLA copolymer exhibited a property for down-regulation of P-gp expression to some extent.

3.8. Effect of HNK/PP-PM on plasma membrane fluidity

Variation of plasma membrane fluidity in MCF-7/ADR cells in the presence of HNK/PP-PM was evaluated by fluorescence polarization method using TMA-DPH as a probe. To validate the fluorescence polarization method for MCF-7/ADR cells, variation in plasma membrane microviscosity in the presence of benzyl alcohol (fluidization agent) [14] was first evaluated. As shown in Fig. 4B, following treatment of MCF-7/ADR cells with benzyl alcohol, extremely significant decrease in plasma membrane microviscosity was observed ($p < 0.001$), which was in accordance with previous report [14]. In addition, the result in the present study has proved that HNK had no significant influence on plasma membrane microviscosity at an incubation period of 48 h. On the contrary, drastic decrease in plasma membrane microviscosity was observed following treatment of MCF-7/ADR cells with either HNK/PP-PM or PEOz-PLA compared with the blank control ($p < 0.001$), while there was no significant difference in reduction in plasma membrane microviscosity for treatment with HNK/PP-PM and PEOz-PLA ($p > 0.05$). These results suggested that PEOz-PLA might play a key role in decrease of plasma membrane microviscosity for HNK/PP-PM.

3.9. MDA-MB-231 cell invasion assay

Prior to assessments of invasion and migration, the cytotoxicity of HNK/PP-PM to MDA-MB-231 cells was evaluated by using the SRB assay in a wide HNK concentration range. Based on the results of cytotoxicity presented in Fig. 5A, HNK/PP-PM at HNK concentration lower than 5 $\mu\text{g/mL}$ was considered not to be toxic to MDA-MB-231 cells.

Cell invasion was a prerequisite in initiating tumor metastasis when tumor cells degrade the extracellular matrix (ECM) and penetrate through blood vessels [45]. The effect of PTX+HNK/PP-PM1 on the invasive ability of MDA-MB-231 cells was therefore first evaluated using Matrigel-coated membrane at the concentration of both HNK and PTX ranging from 0.42 $\mu\text{g/mL}$ to 6.66 $\mu\text{g/mL}$. Treatment with three micelles caused remarkably decreased penetration of MDA-MB-231 cells across the Matrigel-coated membrane compared with the control cells, respectively (Fig. 5B). Moreover, the effect of anti-motility of MDA-MB-231 cells induced by PTX/PP-PM and HNK/PP-PM displayed noticeable concentration-dependence, and no significant difference in anti-motility effect between them was observed at the concentration ranging from 0.83 to 3.33 $\mu\text{g/mL}$ ($p > 0.05$). As expected, the anti-invasion ability was greatly enhanced by PTX+HNK/PP-PM1 without remarkable drug concentration-dependence, highlighting the benefit of co-delivery of PTX and HNK by PEOz-PLA micelles.

3.10. MDA-MB-231 cell migration assay

To analyze whether PTX+HNK/PP-PM1 could retard the migration of MDA-MB-231 cells, the migration assay using a Transwell was conducted for MDA-MB-231 cells treated with PTX+HNK/PP-

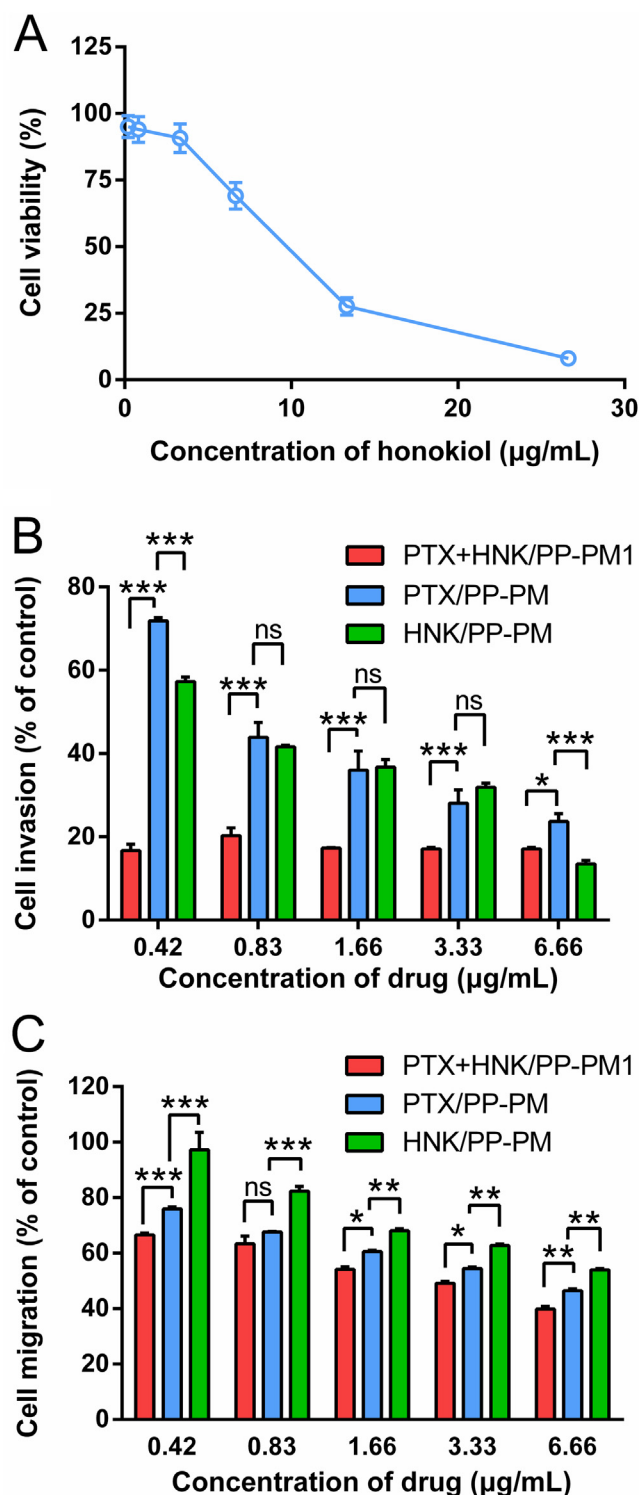


Fig. 5. Cytotoxicity of HNK/PP-PM against MDA-MB-231 cells after incubation for 48 h ($n = 6$) (A). Effect of various drug loaded micelles on MDA-MB-231 cells invasion through Matrigel (B) and migration through polycarbonate filters (C) within 48 h. $^{ns}p > 0.05$, $^*p < 0.05$, $^{**}p < 0.01$, $^{***}p < 0.001$.

PM1 with both HNK and PTX concentration ranging from 0.42 to 6.66 $\mu\text{g/mL}$ for 48 h in comparison with PTX/PP-PM and HNK/PP-PM. In keeping with the migration results, drug concentration-dependent inhibition on cell migration was also found for three micelles in Fig. 5C. Besides, there existed a significant difference in cell migration inhibition between PTX+HNK/PP-PM1 and PTX/PP-PM almost at each tested concentration, and PTX/PP-PM had a

better ability to inhibit cell migration than HNK/PP-PM in the whole tested concentration range. For example, at the lowest drug concentration, the migration of MDA-MB-231 cells decreased to 66.6% for PTX+HNK/PP-PM1, while 75.9% for PTX/PP-PM and 97.3% for HNK/PP-PM. This trend indicated that the co-delivery of PTX and HNK by PEOz-PLA micelles may be beneficial to prevent tumor cell migration.

3.11. Pulmonary metastasis inhibition

Inhibition of various micelle formulations on *in vivo* pulmonary metastasis was finally estimated in nude mice intravenously given MDA-MB-231-luc-GFP cells. To visually observe the situation of tumor metastasis, the bioluminescence imaging system was used here because it provides a real-time and sensitive analysis for multiple tissues, and is especially advantageous in evaluating the inhibition of tumor metastasis. As shown in Fig. 6A, a more intense bioluminescence signal was observed in lung tissue for saline group and HNK/PP-PM compared with PTX/PP-PM and PTX+HNK/PP-PM1, respectively. Furthermore, the bioluminescence in lung tissue for PTX/PP-PM and PTX+HNK/PP-PM1 was also distinct from each other. As expected, PTX+HNK/PP-PM1 produced a weaker bioluminescence signal in lung tissue compared with PTX/PP-PM, and the bioluminescence signal in lung tissue for PTX/PP-PM was remarkably weaker than that for HNK/PP-PM. Further, the quantification analysis results showed that bioluminescence intensity of *in situ* lung was greater than 65% of total in mice for all tested samples (Fig. 6B), revealing that many tumor cells were most likely to metastasize to lungs. These suggested that the lung was the main site of metastasis via injection of MDA-MB-231-luc-GFP cells into the tail vein, which was in agreement with previous reports [38,46].

The superiority of PTX+HNK/PP-PM1 in prevention of lung metastasis was further confirmed by images of the excised lungs. The *ex vivo* imaging (Fig. 6C) revealed that intense bioluminescence signal could be detected in the lung of saline and HNK/PP-PM group. In keeping with bioluminescence images of *in situ* lungs (Fig. 6A), bioluminescence signal of *ex vivo* lungs ranked as saline \approx HNK/PP-PM > PTX/PP-PM > PTX+HNK/PP-PM1 (Fig. 6D). Stronger bioluminescence signals indicated more serious metastasis. These were further evidenced by H&E staining shown in Fig. 6E. Obviously, there existed large tumor metastasis locus (black arrow) in the lung for saline and HNK/PP-PM, while almost no tumor metastasis locus was observed for PTX/PP-PM and PTX+HNK/PP-PM1. These suggested that the pulmonary metastasis inhibition efficiency of PTX+HNK/PP-PM1 was superior to that of PTX/PP-PM.

On the other hand, lung/body coefficient, i.e. the ratio of lung weight to body weight, for PTX+HNK/PP-PM1 group was extremely closest to 0.7%, normal value for normal mice [47], compared with the other three groups, and PTX/PP-PM the next (Fig. 6F). Taken together, it could be concluded that the tumor pulmonary metastasis inhibition efficacy of combination of PTX with HNK was superior to PTX alone although HNK/PP-PM had almost no better behavior than the saline group, which might be attributed to low dose of HNK.

4. Discussion

We developed dual drug-loaded pH-responsive polymeric micelles based on PEOz-PLA for both anti-MDR and anti-metastasis, and elucidated their action mechanisms of modulation MDR. The developed micelles were anticipated to take advantages of pH-sensitivity of PEOz-PLA micelles, and antitumor effect of PTX

as well as inhibition effect of P-gp mediated efflux and tumor metastasis of HNK to improve antitumor efficacy of PTX.

As known, physicochemical characteristics are of prime importance for developing efficient nanoparticles to deliver antitumor drugs due to the fact that the physicochemical properties of nanoparticles significantly influence the *in vitro* and *in vivo* performance of the encapsulated drugs. In the present work, nanosized PTX+HNK/PP-PM was constructed and characterized (Fig. 1), which might show higher accumulation at tumor sites due to their reduction in clearance by the reticuloendothelial system, their passive tumor targeting through EPR effect and pH-sensitivity (Fig. 2) [12], and rapid escape from endo/lysosomes (Fig. 2) [31] to evidently enhance intracellular free drug concentration in a short time and thereby synergistically and efficiently kill tumor cells by the two drugs. Hence, pH-responsive polymeric micelles are believed to be of particular interest for intracellular drug delivery [48]. Nevertheless, this pH-dependent release characteristic of PEOz-PLA micelles is something of a mystery as tertiary amide moieties present in PEO segments are very little basic and cannot be protonated close to neutral pH. However, the partial hydrolysis of amide groups (the side chains) of purified PEOz and PEOz-PLA to form secondary amine groups during titration (Figs. S3 and S4) and drug release at pH 5.0 (Figs. S5 and S6) was evidenced not to occur by ^1H NMR spectra obtained for the polymers following titration and drug release. Therefore, the mechanism for pH-responsivity of PEOz-PLA micelles is not clear and requires further investigations.

MDR has been considered to be a major hurdle to the successful chemotherapy of cancer and generally results from the overexpression of P-gp in tumor cells [49]. P-gp is able to pump various drugs out of cells, thus leading to a reduction in intracellular concentration of drugs to below toxic levels and then limiting the cytotoxicity of drugs [50]. For this reason, one of the rational strategies to overcome MDR is to alleviate the drug efflux by inhibiting P-gp through co-delivery of antitumor drug and P-gp inhibitor. The comprehensive results of cytotoxicity (Fig. 3C and Table 2) and cellular uptake (Fig. 3D) indicated stronger MDR reversal effect of PTX+HNK/PP-PM1 with 1:1 mass ratio of PTX to HNK. Notably, HNK had no cytotoxicity in the tested concentration range (Fig. 3B), meaning that the enhancement of cytotoxicity of PTX+HNK/PP-PM1 compared with PTX/PP-PM was assigned to the reduction of cellular export rather than the cytotoxicity of HNK. In addition, a synergistic effect for MDR reversal might be provided by pH-sensitive polymeric micelles and their components. The results in the present study and in our previous work demonstrated such combined effect. Firstly, polymeric micelles may alter drug uptake in tumor cells. In general, free drugs enter tumor cells through passive diffusion and are easily recognized by the efflux pumps located on the cell membrane or captured by ABC transporter proteins, whereas drugs encapsulated in polymeric micelles are internalized through endocytosis and may avoid identification by the efflux pumps, thus leading to increased intracellular accumulation of drugs [51]. Further, quick drug release triggered by pH for pH-responsive polymeric micelles may remarkably enhance the intracellular free drug concentration in a short time and thereby efficiently kill tumor cells [52]. Moreover, a number of block copolymers have been demonstrated to exhibit the activity of P-gp efflux inhibition [13–15]. This was further confirmed by the results that PEOz-PLA could increase plasma membrane fluidity and down-regulate P-gp expression (Fig. 4).

In order to elucidate the possible reasons for enhanced cytotoxicity against MCF-7/ADR cells (Fig. 3C and Table 2) and cellular uptake (Fig. 3D) by PTX+HNK/PP-PM, the related mechanism was explored in detail. Our mechanistic studies provided important convincing evidences for possible inhibition mechanism of P-gp efflux by HNK/PP-PM based on the results of their ability to

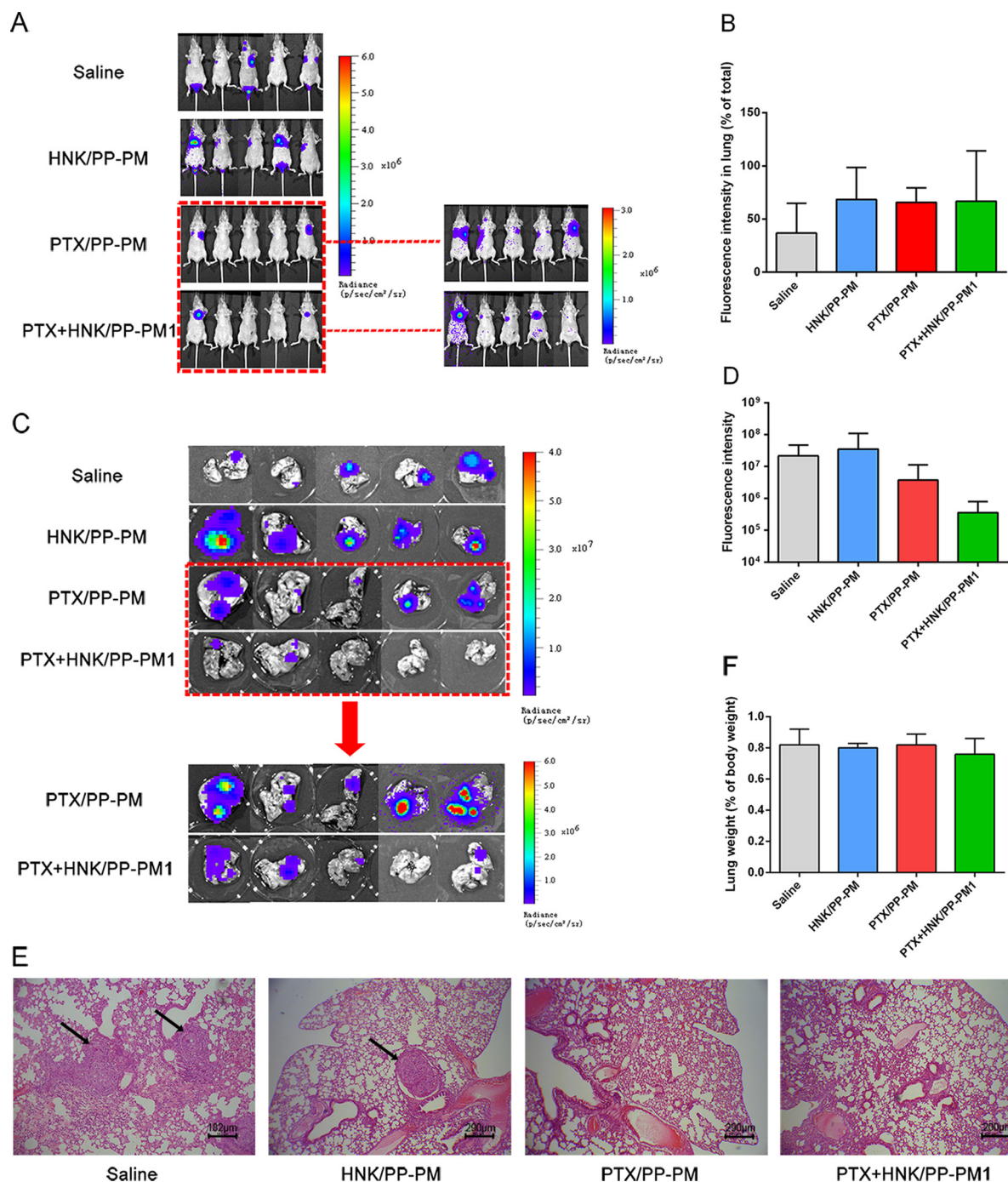


Fig. 6. (A) *In vivo* bioluminescent images of mice treated with saline, HNK/PP-PM, PTX/PP-PM and PTX+HNK/PP-PM1 given equivalent doses of PTX at 25 mg/kg and HNK at 25 mg/kg, respectively ($n = 5$). The images marked with red dotted lines were called out for easy comparison under another scale bar. (B) The bioluminescence intensity of *in situ* lungs in mice treated with various formulations. (C) *Ex vivo* bioluminescent images of the excised lungs for mice treated with various formulations. The images marked with red dotted lines were called out for easy comparison under another scale bar. (D) The bioluminescence intensity of *ex vivo* lungs in mice treated with various formulations. (E) Representative micrographs of lung sections stained with H&E. (F) The wet weight of lung for mice treated with various formulations. (For interpretation of the references to colour in this figure legend, the reader is referred to the web version of this article.)

down-regulate P-gp expression and increase plasma membrane fluidity which induced changes in P-gp conformation and ATPase activity [53]. These parameters were selected according to previous reports showing that the effects of HNK [23,24] and PEG-PLA [13] on P-gp efflux activity are related to down-regulation of P-gp expression for HNK through inhibiting the activity of NF-kappa B and alteration of membrane fluidity for PEG-PLA. These were further confirmed by the present findings that HNK could down-regulate P-gp expression (Fig. 4A) without alteration in

plasma membrane fluidity (Fig. 4B) in MCF-7/ADR cells, whereas PEOz-PLA could slightly down-regulate P-gp expression (Fig. 4A) besides increased plasma membrane fluidity (Fig. 4B). Consequently, HNK/PP-PM integrated the merits of HNK for its down-regulation of P-gp expression (Fig. 4A) and PEOz-PLA for its increase in plasma membrane fluidity (Fig. 4B). Hence, the possible mechanisms of P-gp efflux inhibition for HNK/PP-PM appeared to be related to down-regulation of P-gp expression and increase in plasma membrane fluidity, which are commonly reported to be

the two major contributors to P-gp efflux inhibition mediated by P-gp inhibitors. Overall, the developed dual drug-loaded micelles could efficiently deliver PTX to the drug resistant cells and enhance the pharmacological activity of PTX. Thus, the micelles in the present study would be a potential Cremophore EL-free delivery system for PTX. The study regarding antitumor efficacy *in vivo* will be further conducted to fully characterize the nature of overcoming MDR effect of the dual drug-loaded micelles.

On the other hand, cancer metastasis accounts for 90% of cancer-associated deaths [54]. Currently, majority of nanotechnology-based cancer therapies have focused on the treatment of primary tumors in the past few years, prevention or reduction of the incidence of metastasis at the same time of chemotherapy should not be overlooked accordingly. As known, metastasis is a highly complex process including progressive proliferation of cancer cells and vascularization, local invasion through veins, penetration into the circulation, settlement and growth as secondary tumor [55,56]. Tumor cell invasion and migration from a primary tumor to seed secondary tumors in distant sites are considered to be major events in metastatic cascade [13]. Moreover, it is well known that there existed a mutual relationship between formation of metastasis and MMPs (matrix metalloproteinases) family, and two important family members MMP-2 and MMP-9 involved in tumor invasion and migration [57,58]. Previous documents reported that HNK may remarkably decrease the expression of MMP-2 and MMP-9 in tumor cells induced by TNF- α , NF- κ B activation, and ERK1/2 phosphorylation [59], inhibit the phosphorylation of STAT3 [60] and activate the PI3K/Akt/mTOR and ERS/ROS/ERK1/2 signaling pathways [61], and PTX may suppress tumor metastasis by inhibiting the expression of EGFR and MMPs [62–64]. Enlightened by these, we therefore set out to examine the hypothesis that co-delivery of PTX and HNK by PEOz-PLA micelles might present favorable and collaborative anti-metastasis efficacy. Having verified the stronger synergetic MDR reversal effect of PTX+HNK/PP-PM1 *in vitro*, the anti-metastasis efficacy of PTX+HNK/PP-PM1 was further evidenced by first evaluating the effect of PTX+HNK/PP-PM1 on invasion and migration of MDA-MB-231 cells. We really observed a reproducible, but modest, inhibition effect of HNK/PP-PM on invasion and migration of MDA-MB-231 cells and anti-invasion effect was obviously stronger than anti-migration effect (Fig. 5B and C). These effects presented a strong dependence on HNK concentration, and were not based on cytotoxicity of HNK/PP-PM due to the fact that HNK/PP-PM had almost no cytotoxicity at HNK concentration lower than 5 μ g/mL (Fig. 5A). Further, in the tested concentration range, PTX/PP-PM exhibited comparative inhibition effect on invasion to HNK/PP-PM and highly significantly stronger inhibition effect on migration of MDA-MB-231 cells than HNK/PP-PM. Excitedly, a substantial inhibition of PTX+HNK/PP-PM1 on invasion of MDA-MB-231 cells was evidenced and kept low and almost constant level in the whole drug concentration range, suggesting that the highly effective inhibition on cell invasion was available for PTX+HNK/PP-PM1 even at low drug dose. This collaborative effect was also observed in migration results (Fig. 5C) although anti-migration effect of PTX+HNK/PP-PM1 was inferior to its anti-invasion effect. More importantly, based on the results of effects of intravenously injected PTX+HNK/PP-PM1 on bioluminescence intensity of *in situ* and *ex vivo* lungs, condition of lung histopathology and lung/body coefficient for mice (Fig. 6), *in vivo* bioluminescence images directly monitoring tumor metastasis burden further provided convincing evidences for substantial suppression of tumor metastasis by PTX+HNK/PP-PM1 compared with PTX/PP-PM. Nevertheless, to gain further insight into the role of PTX+HNK/PP-PM1 in anti-tumor metastasis activity, more investigations are required to explore how PTX+HNK/PP-PM1 inhibits the tumor metastasis and what the optimal dose of the two drugs is. Taken together, we demon-

strated the ability of PTX+HNK/PP-PM1 to prevent the development of the metastasis, suggesting the potential of the micelles to target early-stage breast cancer.

5. Conclusions

In current study, PTX and HNK were efficiently encapsulated into PEOz-PLA micelles. The dual drug-loaded PEOz-PLA micelles were characterized by small size and high drug encapsulation efficiency, and their favorable pH-dependent drug release characteristics were evidenced. Synergistically enhanced cellular uptake and cytotoxicity to MCF-7/ADR suggested the benefit of co-delivery of PTX and HNK by pH-responsive polymeric micelles for overcoming MDR. Mechanistic studies demonstrated that decrease of plasma membrane microviscosity and down-regulation of P-gp expression might be mainly responsible for inhibition of P-gp efflux for PTX+HNK/PP-PM1. And what's more, PTX+HNK/PP-PM1 was further demonstrated to be able to suppress the development of tumor cell invasion and migration. Our study thus offered a new strategy to treat MDR cancer and prevent tumor metastasis via PTX in combination with HNK delivered by pH-sensitive polymeric micelles.

Conflicts of interest

The authors declare no conflicts of interests.

Acknowledgements

This research was financially supported by the National Natural Science Foundation of China (No. 81673366) and the National Key Science Research Program of China (973 Program, 2015CB932100).

Appendix A. Supplementary data

Supplementary data associated with this article can be found, in the online version, at <http://dx.doi.org/10.1016/j.actbio.2017.08.027>.

References

- [1] D. Elias, F. Blot, O.A. El, S. Antoun, P. Lasser, V. Boige, P. Rougier, M. Ducreux, Curative treatment of peritoneal carcinomatosis arising from colorectal cancer by complete resection and intraperitoneal chemotherapy, *Cancer* 92 (2001) 71–76.
- [2] M.M. Gottesman, V. Ling, The molecular basis of multidrug resistance in cancer: the early years of P-glycoprotein research, *FEBS Lett.* 580 (2006) 998–1009.
- [3] C.H. Choi, ABC transporters as multidrug resistance mechanisms and the development of chemosensitizers for their reversal, *Cancer Cell Int.* 5 (2005) 30.
- [4] X. Duan, J. Xiao, Q. Yin, Z. Zhang, H. Yu, S. Mao, Y. Li, Smart pH-sensitive and temporal-controlled polymeric micelles for effective combination therapy of doxorubicin and disulfiram, *ACS Nano* 7 (2013) 5858–5869.
- [5] A. Palmeira, E. Sousa, M.H. Vasconcelos, M.M. Pinto, Three decades of P-gp inhibitors: skimming through several generations and scaffolds, *Curr. Med. Chem.* 19 (2012) 1946–2025.
- [6] T. Fojo, S. Bates, Strategies for reversing drug resistance, *Oncogene* 22 (2003) 7512–7723.
- [7] S. Nobili, I. Landini, B. Giglioli, E. Mini, Pharmacological strategies for overcoming multidrug resistance, *Curr. Drug Targets* 7 (2006) 861–879.
- [8] S. Kapse-Mistry, T. Govender, R. Srivastava, M. Yegeri, Nanodrug delivery in reversing multidrug resistance in cancer cells, *Front. Pharmacol.* 5 (2014) 159.
- [9] F. Wang, Y.C. Wang, S. Dou, M.H. Xiong, T.M. Sun, J. Wang, Doxorubicin-tethered responsive gold nanoparticles facilitate intracellular drug delivery for overcoming multidrug resistance in cancer cells, *ACS Nano* 5 (2011) 3679–3692.
- [10] C.M. Hu, L. Zhang, Therapeutic nanoparticles to combat cancer drug resistance, *Curr. Drug Metab.* 10 (2009) 836–841.
- [11] X. Li, P. Li, Y. Zhang, Y. Zhou, X. Chen, Y. Huang, Y. Liu, Novel mixed polymeric micelles for enhancing delivery of anticancer drug and overcoming multidrug resistance in tumor cell lines simultaneously, *Pharm. Res.* 27 (2010) 1498–1511.

- [12] Y. Zhao, Y. Zhou, D. Wang, Y. Gao, J. Li, S. Ma, L. Zhao, C. Zhang, Y. Liu, X. Li, pH-responsive polymeric micelles based on poly(2-ethyl-2-oxazoline)-poly(D, L-lactide) for tumor-targeting and controlled delivery of doxorubicin and P-glycoprotein inhibitor, *Acta Biomater.* 17 (2015) 182–192.
- [13] W. Li, X. Li, Y. Gao, Y. Zhou, S. Ma, Y. Zhao, J. Li, Y. Liu, X. Wang, D. Yin, Inhibition mechanism of P-glycoprotein mediated efflux by mPEG-PLA and influence of PLA chain length on P-glycoprotein inhibition activity, *Mol. Pharm.* 11 (2014) 71–80.
- [14] J. Zastre, J.K. Jackson, W. Wong, H.M. Burt, Methoxypolyethylene glycol-block-polycaprolactone diblock copolymers reduce P-glycoprotein efflux in the absence of a membrane fluidization effect while stimulating P-glycoprotein ATPase activity, *J. Pharm. Sci.* 96 (2007) 864–875.
- [15] J.A. Zastre, J.K. Jackson, W. Wong, H.M. Burt, P-glycoprotein efflux inhibition by amphiphilic diblock copolymers: relationship between copolymer concentration and substrate hydrophobicity, *Mol. Pharm.* 5 (2008) 643–653.
- [16] W. Zou, C. Sarisozen, V.P. Torchilin, The reversal of multidrug resistance in ovarian carcinoma cells by co-application of tariquidar and paclitaxel in transferrin-targeted polymeric micelles, *J. Drug Target.* 25 (2017) 225–234.
- [17] K.A. Hoadley, M.B. Siegel, K.L. Kanchi, C.A. Miller, L. Ding, W. Zhao, X. He, J.S. Parker, M.C. Wendl, R.S. Fulton, R.T. Demeter, R.K. Wilson, L.A. Carey, C.M. Perou, E.R. Mardis, Tumor evolution in two patients with basal-like breast cancer: a retrospective genomics study of multiple metastases, *PLoS Med.* 13 (2016) e1002174.
- [18] E.A. Murphy, B.K. Majeti, L.A. Barnes, M. Makale, S.M. Weis, K. Lutu-Fuga, W. Wrasidlo, D.A. Cheresh, Nanoparticle-mediated drug delivery to tumor vasculature suppresses metastasis, *Proc. Natl. Acad. Sci. U.S.A.* 105 (2008) 9343–9348.
- [19] A. Schroeder, D.A. Heller, M.M. Winslow, J.E. Dahlman, G.W. Pratt, R. Langer, T. Jacks, D.G. Anderson, Treating metastatic cancer with nanotechnology, *Nat. Rev. Cancer* 12 (2011) 39–50.
- [20] M. Karaca, R. Dutta, Y. Ozsoy, R.I. Mahato, Micelle mixtures for coadministration of gemcitabine and GDC-0449 to treat pancreatic cancer, *Mol. Pharm.* 13 (2016) 1822–1832.
- [21] R. van Sluis, Z.M. Bhujwalla, N. Raghunand, P. Ballesteros, J. Alvarez, S. Cerdan, J.P. Galons, R.J. Gillies, In vivo imaging of extracellular pH using ¹H MRSI, *Magn. Reson. Med.* 41 (1999) 743–750.
- [22] I. Mellman, R. Fuchs, A. Helenius, Acidification of the endocytic and exocytic pathways, *Annu. Rev. Biochem.* 55 (1986) 663–700.
- [23] D. Xu, Q. Lu, X. Hu, Down-regulation of P-glycoprotein expression in MDR breast cancer cell MCF-7/ADR by honokiol, *Cancer Lett.* 243 (2006) 274–280.
- [24] Y. Chen, X. Wang, C. Duan, J. Chen, M. Su, Y. Jin, Y. Deng, D. Wang, C. Chen, L. Zhou, J. Cheng, W. Wang, Q. Xi, Loss of TAB3 expression by shRNA exhibits suppressive bioactivity and increased chemical sensitivity of ovarian cancer cell lines via the NF-kappaB pathway, *Cell Prolif.* 49 (2016) 657–668.
- [25] Y.J. Chen, C.L. Wu, J.F. Liu, Y.C. Fong, S.F. Hsu, T.M. Li, Y.C. Su, S.H. Liu, C.H. Tang, Honokiol induces cell apoptosis in human chondrosarcoma cells through mitochondrial dysfunction and endoplasmic reticulum stress, *Cancer Lett.* 291 (2010) 20–30.
- [26] T.E. Battle, J. Arbiser, D.A. Frank, The natural product honokiol induces caspase-dependent apoptosis in B-cell chronic lymphocytic leukemia (B-CLL) cells, *Blood* 106 (2005) 690–697.
- [27] S. Cheng, Y. Castillo, I. Eliaz, D. Sliva, Honokiol suppresses metastasis of renal cell carcinoma by targeting KISS1/KISS1R signaling, *Int. J. Oncol.* 46 (2015) 2293–2298.
- [28] T. Nabekura, T. Hiroi, T. Kawasaki, Y. Uwai, Effects of natural nuclear factor-kappa B inhibitors on anticancer drug efflux transporter human P-glycoprotein, *Biomed. Pharmacother.* 70 (2015) 140–145.
- [29] D. Wang, Y. Zhou, X. Li, X. Qu, Y. Deng, Z. Wang, C. He, Y. Zou, Y. Jin, Y. Liu, Mechanisms of pH-sensitivity and cellular internalization of PEO₂-b-PLA micelles with varied hydrophilic/hydrophobic ratios and intracellular trafficking routes and fate of the copolymer, *ACS Appl. Mater. Interfaces* 9 (2017) 6916–6930.
- [30] X. Li, Z. Yang, K. Yang, Y. Zhou, X. Chen, Y. Zhang, F. Wang, Y. Liu, L. Ren, Self-assembled polymeric micellar nanoparticles as nanocarriers for poorly soluble anticancer drug etahaselen, *Nanoscale Res. Lett.* 4 (2009) 1502–1511.
- [31] Y. Gao, Y. Li, Y. Li, L. Yuan, Y. Zhou, J. Li, L. Zhao, C. Zhang, X. Li, Y. Liu, PSMA-mediated endosome escape-accelerating polymeric micelles for targeted therapy of prostate cancer and the real time tracing of their intracellular trafficking, *Nanoscale* 7 (2015) 597–612.
- [32] Y. Gao, Y. Zhou, L. Zhao, C. Zhang, Y. Li, J. Li, X. Li, Y. Liu, Enhanced antitumor efficacy by cyclic RGDK-conjugated and paclitaxel-loaded pH-responsive polymeric micelles, *Acta Biomater.* 23 (2015) 127–135.
- [33] N. Li, X.R. Li, Y.X. Zhou, W.J. Li, Y. Zhao, S.J. Ma, J.W. Li, Y.J. Gao, Y. Liu, X.L. Wang, D.D. Yin, The use of polyion complex micelles to enhance the oral delivery of salmon calcitonin and transport mechanism across the intestinal epithelial barrier, *Biomaterials* 33 (2012) 8881–8892.
- [34] B. Chazotte, Labeling the plasma membrane with TMA-DPH, *Cold Spring Harb. Protoc.* 2011 (2011). [pdb.prot5622](http://dx.doi.org/10.1101/05622).
- [35] M. Shinitzky, Y. Barenholz, Fluidity parameters of lipid regions determined by fluorescence polarization, *Biochim. Biophys. Acta* 515 (1978) 367–394.
- [36] S. Kanda, M. Kuzuya, M.A. Ramos, T. Koike, K. Yoshino, S. Ikeda, A. Iguchi, Matrix metalloproteinase and alphavbeta3 integrin-dependent vascular smooth muscle cell invasion through a type I collagen lattice, *Arterioscler. Thromb. Vasc. Biol.* 20 (2000) 998–1005.
- [37] S. Boyden, The chemotactic effect of mixtures of antibody and antigen on polymorphonuclear leucocytes, *J. Exp. Med.* 115 (1962) 453–466.
- [38] Z. Wang, Y. Yu, W. Dai, J. Cui, H. Wu, L. Yuan, H. Zhang, X. Wang, J. Wang, X. Zhang, Q. Zhang, A specific peptide ligand-modified lipid nanoparticle carrier for the inhibition of tumor metastasis growth, *Biomaterials* 34 (2013) 756–764.
- [39] C. Henriques, A. Henriques-Pons, M. Meuser-Batista, A.S. Ribeiro, W. de Souza, In vivo imaging of mice infected with bioluminescent *Trypanosoma cruzi* unveils novel sites of infection, *Parasit. Vectors* 7 (2014) 89.
- [40] D. Peer, J.M. Karp, S. Hong, O.C. Farokhzad, R. Margalit, R. Langer, Nanocarriers as an emerging platform for cancer therapy, *Nat. Nanotechnol.* 2 (2007) 751–760.
- [41] Z.G. Gao, A.N. Lukyanov, A. Singhal, V.P. Torchilin, Diacyllipid-polymer micelles as nanocarriers for poorly soluble anticancer drugs, *Nano Lett.* 2 (2002) 979–982.
- [42] J. Liu, Y. Xiao, C. Allen, Polymer-drug compatibility: a guide to the development of delivery systems for the anticancer agent, ellipticine, *J. Pharm. Sci.* 93 (2004) 132–143.
- [43] T.C. Chou, P. Talalay, Quantitative analysis of dose-effect relationships: the combined effects of multiple drugs or enzyme inhibitors, *Adv. Enzyme Regul.* 22 (1984) 27–55.
- [44] C.P. Reynolds, B.J. Maurer, Evaluating response to antineoplastic drug combinations in tissue culture models, *Methods Mol. Med.* 110 (2005) 173–183.
- [45] F. van Zijl, G. Krupitza, W. Mikulits, Initial steps of metastasis: cell invasion and endothelial transmigration, *Mutat. Res.* 728 (2011) 23–34.
- [46] M.M. Richert, P.A. Phadke, G. Matters, D.J. DiGirolamo, S. Washington, L.M. Demers, J.S. Bond, A. Manni, D.R. Welch, Metastasis of hormone-independent breast cancer to lung and bone is decreased by alpha-difluoromethylornithine treatment, *Breast Cancer Res.* 7 (2005) R819–R827.
- [47] X.Y. Zhang, C.L. Zhan, Y.H. Xiao, X.G. Tang, Measurement and comparisons of organ weight, organ coefficient, hematological parameters and hematological biochemical parameters of specific pathogen free Balb/c mice, *J. Clin. Rehabilitative Tissue Eng. Res.* 15 (2011) 7734–7737.
- [48] H. Wu, L. Zhu, V.P. Torchilin, pH-sensitive poly(histidine)-PEG/DSPE-PEG copolymer micelles for cytosolic drug delivery, *Biomaterials* 34 (2013) 1213–1222.
- [49] M.M. Gottesman, Mechanisms of cancer drug resistance, *Annu. Rev. Med.* 53 (2002) 615–627.
- [50] T.W. Loo, D.M. Clarke, Location of the rhodamine-binding site in the human multidrug resistance P-glycoprotein, *J. Biol. Chem.* 277 (2002) 44332–44338.
- [51] A.R. Kirtane, S.M. Kalscheuer, J. Panyam, Exploiting nanotechnology to overcome tumor drug resistance: Challenges and opportunities, *Adv. Drug Deliv. Rev.* 65 (2013) 1731–1747.
- [52] C.H. Wang, C.H. Wang, G.H. Hsiue, Polymeric micelles with a pH-responsive structure as intracellular drug carriers, *J. Control. Release* 108 (2005) 140–149.
- [53] R. Regev, Y.G. Assaraf, G.D. Eytan, Membrane fluidization by ether, other anesthetics, and certain agents abolishes P-glycoprotein ATPase activity and modulates efflux from multidrug-resistant cells, *Eur. J. Biochem.* 259 (1999) 18–24.
- [54] D. Hanahan, R.A. Weinberg, The hallmarks of cancer, *Cell* 100 (2000) 57–70.
- [55] S. Menashi, M. Dehem, I. Souliac, Y. Legrand, R. Fridman, Density-dependent regulation of cell-surface association of matrix metalloproteinase-2 (MMP-2) in breast-carcinoma cells, *Int. J. Cancer* 75 (1998) 259–265.
- [56] B. Fayard, F. Bianchi, J. Dey, E. Moreno, S. Djaffer, N.E. Hynes, D. Monard, The serine protease inhibitor protease nexin-1 controls mammary cancer metastasis through LRP-1-mediated MMP-9 expression, *Cancer Res.* 69 (2009) 5690–5698.
- [57] A. Stahl, B.M. Mueller, Binding of urokinase to its receptor promotes migration and invasion of human melanoma cells in vitro, *Cancer Res.* 54 (1994) 3066–3071.
- [58] A.R. Farina, A. Coppa, A. Tiberio, A. Tacconelli, A. Turco, G. Colletta, A. Gulino, A. R. Mackay, Transforming growth factor-beta1 enhances the invasiveness of human MDA-MB-231 breast cancer cells by up-regulating urokinase activity, *Int. J. Cancer* 75 (1998) 721–730.
- [59] X. Zhu, Z. Wang, C. Hu, Z. Li, J. Hu, Honokiol suppresses TNF-alpha-induced migration and matrix metalloproteinase expression by blocking NF-kappaB activation via the ERK signaling pathway in rat aortic smooth muscle cells, *Acta Histochem.* 116 (2014) 588–595.
- [60] P.S. Yeh, W. Wang, Y.A. Chang, C.J. Lin, J.J. Wang, R.M. Chen, Honokiol induces autophagy of neuroblastoma cells through activating the PI3 K/Akt/mTOR and endoplasmic reticular stress/ERK1/2 signaling pathways and suppressing cell migration, *Cancer Lett.* 370 (2016) 66–77.
- [61] G.J. Wu, C.J. Lin, Y.W. Lin, R.M. Chen, Data analyses of honokiol-induced autophagy of human glioma cells in vitro and in vivo, *Data Brief.* 9 (2016) 667–672.
- [62] M.M. Sayed-Ahmad, M.A. Mohamad, Contribution of nitric oxide and epidermal growth factor receptor in anti-metastatic potential of paclitaxel in human liver cancer cell (HepG2), *J. Egypt. Natl. Canc. Inst.* 17 (2005) 35–41.
- [63] A. Westerlind, E. Hujanen, M. Hoyhtya, U. Puustola, T. Turpeenniemi-Hujanen, Ovarian cancer cell invasion is inhibited by paclitaxel, *Clin. Exp. Metastasis* 15 (1997) 318–328.
- [64] Y. Zhang, H. Zhang, W. Wu, F. Zhang, S. Liu, R. Wang, Y. Sun, T. Tong, X. Jing, Folate-targeted paclitaxel-conjugated polymeric micelles inhibits pulmonary metastatic hepatoma in experimental murine H22 metastasis models, *Int. J. Nanomed.* 9 (2014) 2019–2030.